Comparative performance of seismically deficient exterior beam-column sub-assemblages of different design evolutions: A closer perspective

A. Kanchana Devi[*1,2] and K. Ramanjaneyulu[1,2a]

[1]*CSIR-Structural Engineering Research Centre, Chennai, 600113, Tamil Nadu, India*
[2]*Academy of Scientific and Innovative Research (AcSIR), Chennai, 600113, Tamil Nadu, India*

Abstract. In the present study, exterior beam column sub-assemblages are designed in accordance with the codal stipulations prevailed at different times prior to the introduction of modern seismic provisions, viz., i) Gravity load designed with straight bar anchorage (SP1), ii) Gravity load designed with compression anchorage (SP1-D), iii) designed for seismic load but not detailed for ductility (SP2), and iv) designed for seismic load and detailed for ductility (SP3). Comparative seismic performance of these exterior beam-column sub-assemblages are evaluated through experimental investigations carried out under repeated reverse cyclic loading. Seismic performance parameters like load-displacement hysteresis behavior, energy dissipation, strength and stiffness degradation, and joint shear deformation of the specimens are evaluated. It is found from the experimental studies that with the evolution of the design methods, from gravity load designed to non-ductile and then to ductile detailed specimens, a marked improvement in damage resilience is observed. The gravity load designed specimens SP1 and SP1-D respectively dissipated only one-tenth and one-sixth of the energy dissipated by SP3. The specimen SP3 showcased tremendous improvement in the energy dissipation capacity of nearly 2.56 times that of SP2. Irrespective of the level of design and detailing, energy dissipation is finally manifested through the damage in the joint region. The present study underlines the seismic deficiency of beam-column sub-assemblages of different design evolutions and highlights the need for their strengthening/retrofit to make them fit for seismic event.

Keywords: beam-column sub-assemblage; seismic design; ductile detailing; energy dissipation; strength degradation; shear deformation

1. Introduction

For the seismic design of structures, ground shaking is perceived as the lateral load acting on the structure whose magnitude depends upon the weight of structure, natural period, ground acceleration, soil condition, etc. Various international standards, namely, ACI 318 (2011), NZS 3101 (2006), and EC 8 (2004) provide rigorous guidelines for seismic design of framed structures and are recognized globally. Principally, all these codes of practice codified the seismic design philosophy of structures as, to withstand earthquakes smaller than the design basis earthquake without any damage; to withstand design earthquake with non-structural damage; and to prevent collapse of structure under maximum probable earthquake. In order to prevent collapse of structures under extreme seismic event, codes insist on the capacity design philosophies. According to the capacity design philosophy of strong column-weak beam, the flexural failure of beam is preferable as it is ductile mode and is able to dissipate more energy than other failure modes. In order to achieve the desired failure mode and structural performance, different codes of practice prescribe

design and detailing provisions for the critical components to improve ductility of structure and to avoid brittle failure.

The concepts of ductility detailing were recognized globally during late 70s and were incorporated in the codes of practice during late 80s. Megget and Park (1971), Park and Paulay (1973), Blakeley *et al.* (1975), Paulay *et al.* (1978), Park and Yeoh Sik keong (1979), Paulay and Scarpas (1981), Ehsani and Wight (1985) carried out pioneering work for understanding the behavior of this critical structural component under seismic type of loading and thereby suggesting measures for improving the seismic resistance of structural system which in turn lead to development of seismic design philosophies.

There are lot of existing reinforced concrete (RC) structures which were gravity load designed and seismically deficient. The existing in-service non-seismically designed structures underperform during seismic event, due to inadequate reinforcement, improper detailing, and lack of confinement. Hence, several researchers (Aycardi *et al.* 1994, Bracci *et al.* 1995, El-Attar *et al.* 1997, Calvi *et al.* 2001, Pantelides *et al.* 2002, Dhakal *et al.* 2005, Supaviriyakit and Pimanmas 2008, Yavari *et al.* 2013) carried out investigations to evaluate the seismic performance of non-seismically designed structures with different deficiencies, such as use of smooth mild steel reinforcement, joints without transverse reinforcement, beam bars with different types of anchorage detailing, inadequate main reinforcement to cater for seismic forces,

---

*Corresponding author, Ph.D. Student
 E-mail: kanchana@serc.res.in
[a]Ph.D.

and beam and column with lack of confinement. Considerable efforts were also made by the researchers (Murty *et al.* 2003, Bakir 2003, Bindhu 2008, Rajagopal and Prabavathy 2013) to develop various joint detailing techniques to enhance the seismic performance of the structures. Tsonos (2007) assessed the seismic performance of structures designed according to modern seismic codes and highlighted that at times the specimens may suffer severe joint degradation. Masi *et al.* (2013) analyzed the experimental results of gravity load designed and seismic load designed specimens. From the study, two failure modes were observed i) mixed mode involving beam and joint damage, ii) flexural failure involving beam only. It was also observed that mixed mode of failure reduces the deformation capacity. Chun (2014) developed analytical model for determining the transverse reinforcement required for exterior beam-column joints subjected to reverse cyclic loads. This model takes into account the effect of aspect ratio of the joint. Somma *et al.* (2015) used various indices for evaluating the failure modes of the interior beam and column connection and validated their proposed method with 72 experimental tests carried out on beam-column connections. Further, they proposed a joint capacity design approach for ensuring the better performance of the joint. Marthong *et al.* (2016) proposed fragility functions for deficient and retrofitted exterior RC beam-column connections.

From the reported studies, it could be found that many attempts were made to evolve the seismic design philosophies, where type of joint, geometry, type of loading, detailing of reinforcing steel etc. are the parameters. Furthermore, considerable efforts were also made to understand the seismic behavior of deficient structures and also efforts are made to predict the failure modes of deficient structures. However, comprehensive seismic performance assessment of the beam-column sub-assemblages designed according to the evolution of the codal provisions are scarce. Further, in view of new developments in understanding of seismic loading leading to reclassification of seismic risk of locality, increase in seismic risk due to change in topography and existence of deficient structures necessitates the understanding of seismic performance of existing structures that were built at different times and thereby aid in formulating suitable strengthening strategy. Hence, it is essential to evaluate seismic performance of the beam-column sub-assemblages of different design evolutions, which are the critical structural components of existing RC framed structures. Further, detailed studies on the various key seismic response parameters such as energy dissipation, strength & stiffness degradation and shear deformation of joint are required to connect the behavior of the beam-column sub-assemblages with the response parameters. In the present study, an exterior beam-column joint of a residential framed structure is taken up and designed as per the evolutions of the Indian Standards (IS 456 2000, IS 1893 2002, IS13920 1993) that are commonly used in the Indian sub-continent. The study clearly brings out the behavior of seismically deficient vis-à-vis ductile detailed beam-column sub-assemblages and underlines the need for seismic
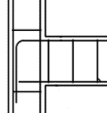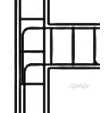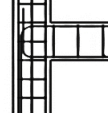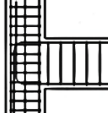
strengthening of deficient structures/structural sub-assemblages. Further, the seismic assessment of these critical components of the structures designed at different times will be a guiding parameter for developing effective strengthening schemes for the deficient ones.

2. Details of beam-column sub-assemblages

An exterior beam-column sub-assemblage (Highlighted in Fig. 1) of typical three storied RC framed building is taken up for study. The geometrical details of the three storied building chosen for this study are as shown in Fig. 1. 3D numerical simulation and analysis of the building frame was carried out. The support conditions are assigned as fixed at the bottom of the column (Fig. 1). The building is analysed for the critical combinations of dead load, live load and seismic load. The moments and shear forces are obtained for different levels of design. Different levels of design as given in Table 1 are considered to evaluate seismic performance of reinforced concrete structures that were constructed in the last 4 to 5 decades. The general dimensions of beam-column sub-assemblage are as follows: overall height of column is 3.8 m, length of column between the centre to centre of hinge is 3.5 mm and length of beam is 1.7 m. The length of beam is arrived based on the point of contra-flexure under the action of combined gravity loads and lateral loads. The lengths of column segments above and below the joint are arrived according to the proportioning of moments at the joint for the combination of loads as shown in Table 2. The cross sectional dimensions adopted for beam and column are 300×400 mm and 300×300 mm respectively. The overall dimensions adopted for the sub-assemblages are as shown in Fig. 2. The reinforcements required for all the specimens are as shown Fig. 3.

The specimens are instrumented extensively by affixing strain gages at critical locations identified on the reinforcement bars. Strain gages are affixed on the main

Table 1 Levels of design considered in the present study

| ID	Design level	Detailing	Remark
SP1	Designed for gravity loads with straight bar anchorage for beam bottom bars		Represents the olden building
SP1-D	Designed for gravity loads with compression anchorage for beam bottom bars		Represents the olden building
SP2	Designed for combination of gravity loads and seismic force, but not provided with ductility detailing		Ordinary Moment Resisting Frame
SP3	Designed for combination of gravity loads and seismic force and provided with code specified ductility detailing		Special Moment Resisting Frame
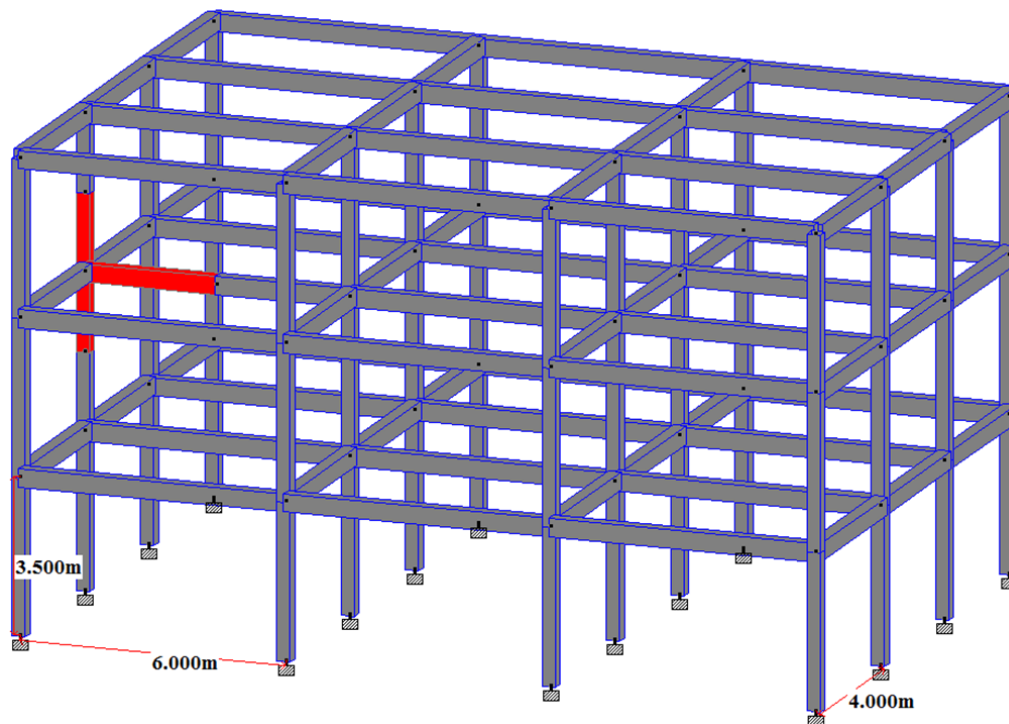
Fig. 1 Geometrical details of building chosen for study

Table 2 Dimensioning of beam-column sub-assemblage

Load Case	Bottom column moment at joint M_B (kNm)	Top column moment at joint (M_t) (kNm)	Beam Moment joint M_u (kNm)	Length of column below joint (m)	Length of column above the joint (m)	Shear generated in test Mu/3.5 (kN)	Shear in bottom column from analysis (kN)	Shear in Top column from analysis(kN)
1.2DL+1.2LL +1.2SL	96.03	64.43	160.68	2.094	1.405	45.910	53.87	40.30
1.5DL+1.5SL	103.69	66.03	168.65	2.138	1.361	48.188	57.84	42.48
0.9DL+1.5SL	62.21	39.62	101.19	2.138	1.361	28.912	48.47	32.96
Average Size				2.1	1.38			

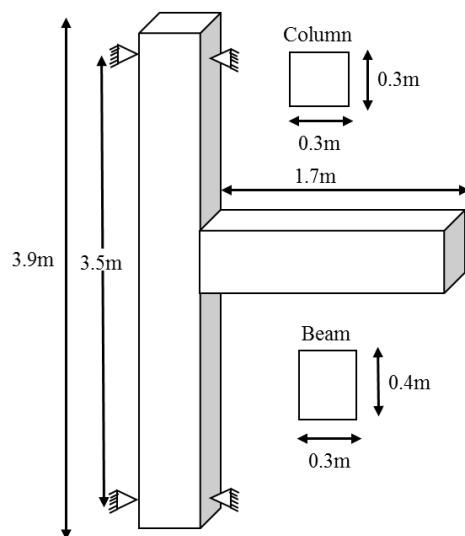* Note: DL - Dead Load; LL - Live Load; SL - Seismic Load

Fig. 2 Dimensions of the sub-assemblage chosen for the study

Table 3(a) Material properties of Concrete

ID	Average concrete cylinder compressive strength at the time of testing (N/mm^2)	Average concrete cylinder split tensile strength at the time of testing (N/mm^2)
SP1	41.34	3.74
SP1-D	41.9	3.59
SP2	39.73	4.15
SP3	40.91	3.88

reinforcement bars of the beam and column, column ties and beam stirrups. The concrete of mix proportions 1:1.695:3.013 with water cement ratio of 0.5 is used. The specimens are cast and cured for 28 days using wet curing. The material properties of steel and concrete used for the study are presented in Table 3.
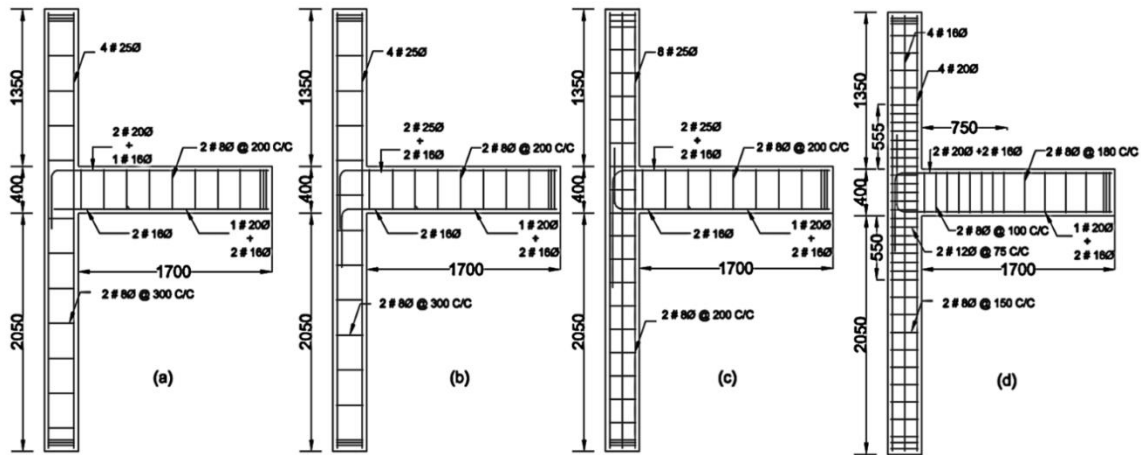
Fig. 3 Reinforcement details of specimen (a) SP1 (b) SP1-D (C) SP2 (d) SP3
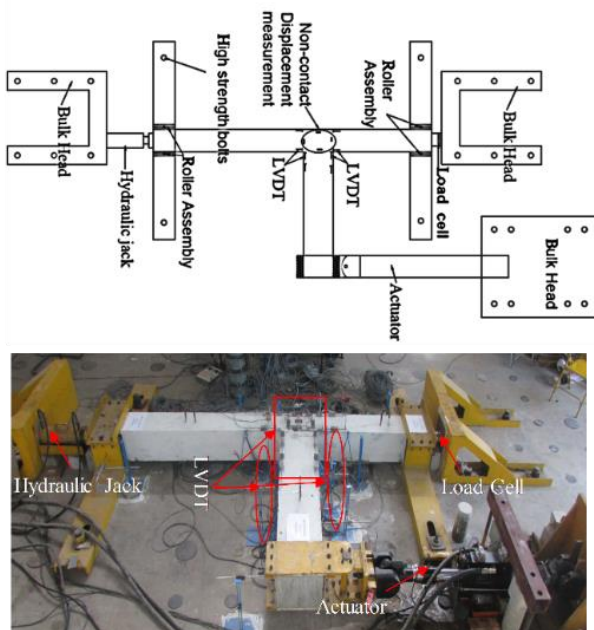

Fig. 4 Instrumentation and set-up for experimental investigations
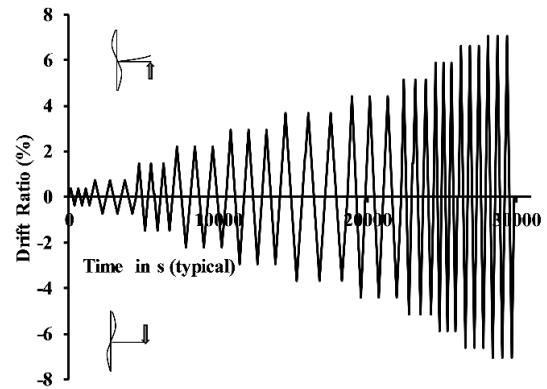

Fig. 5 Reverse cyclic displacement history

Table 3(b) Material properties of steel reinforcement

Diameter of reinforcement (mm)	Average yield strength of steel (N/mm²)	Average ultimate strength of steel (N/mm²)
8	527	641
16	520	647
20	545	621
25	535	643

3. Experimental setup and Investigations

All the test specimens are also instrumented with LVDTs (linear variable displacement transducers), by mounting them on the joint surface and attaching them as well to the beam and the column segments, to measure deflections along the length of beam and column segments and to calculate the shear deformation of the joint. The test setup is arranged on the test floor so that the beam-column joint is positioned horizontally parallel to the test floor and the reverse cyclic load is applied in the plane of the test floor. The schematic diagram of test set-up and actual positioning of test specimen is shown in Fig. 4. An axial load of 300 kN is applied to the column by a hydraulic jack at one end of the column against the reaction block at the other end. The level of axial load (about 10% of the strength) on the column is arrived by analysis of the global system of the three storey three bay building (Fig. 1). The lateral load is applied on the beam tip in displacement control mode using hydraulic actuator of 250 kN capacity, according to the reverse cyclic loading history shown in Fig. 5. Reverse cyclic displacements are applied in terms of drift ratios (%) of the component where the drift ratio is calculated as per Eq. (1).
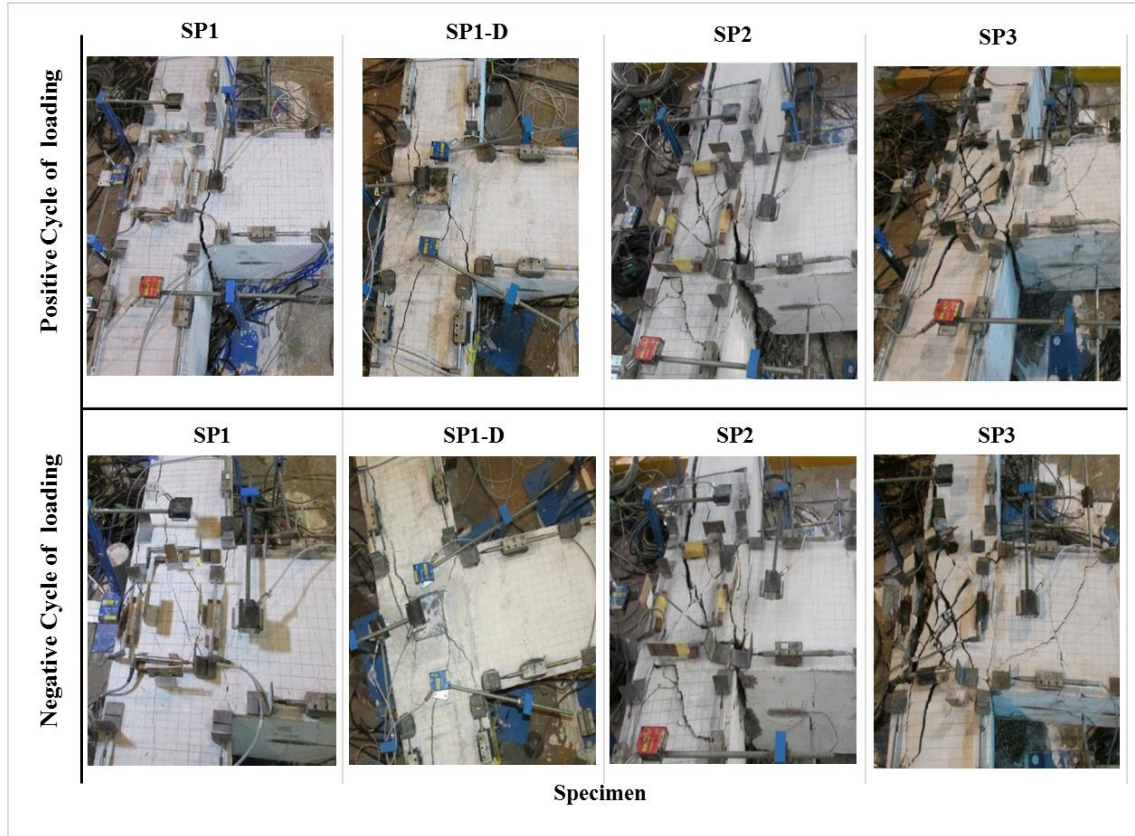
Fig. 6 Crack pattern observed in the specimens at final stage of loading

$$Drift\ ratio(\%) = \frac{\delta}{l_b} \times 100 \qquad (1)$$

Where, δ and l_b are the applied displacement at the beam tip and the length of the beam from column face to the point of application of the displacement respectively.

Three complete cycles are applied for each drift level. Reverse cyclic displacements of equal magnitude are applied on all the specimens, where positive drift or positive cycle produces tension in the beam bottom and negative drift or negative cycle produces tension in beam top. The direction of loading is referred in terms of positive and negative cycles in subsequent sections. The test is stopped when the load either in the positive or negative drift ratio is dropped by approximately 50% of the respective maximum load. The data acquired during the testing of four beam-column sub-assemblages of different design evolutions (SP1, SP1-D, SP2 and SP3) are processed in order to arrive at their responses in terms of seismic performance parameters. The details are presented in the following section.

4. Results and discussion

4.1 Behavior of the specimens

Upon application of displacement at the beam tip in terms of drift ratio, flexural cracks are developed at both top and bottom faces of beam portion of specimen SP1, up to

the drift ratio of +0.737%. At drift ratio of +1.47%, a crack of 3 mm width is developed at the joint due to the absence of proper anchorage of beam bottom reinforcement and the joint crack got widened with increase in drift ratio. At drift ratio of +2.94%, width of the crack at joint is found to be 13 mm and the wide crack is shown in Fig. 6. This behaviour is evident from the strain profiles of beam bottom reinforcement of the gravity load designed specimen SP1 [Fig. 7]. The strain gauge at a distance of 0.2 m from the column centre line is not strained as the length of bar embedded into the joint is insufficient for development of strains. Further, strain values of beam bottom bars indicated that the strains are well below the yield strain of steel throughout the length of the beam and thereby indicating the anchorage failure. During the negative cycles of specimen SP1, upon further increment of drift the major damage is shifted towards the joint region [Fig. 6]. Upon further increment of drift, the joint crack widened in SP1 specimen during negative cycles and this has resulted in huge degradation (i.e., load drop between subsequent drift levels) of global strength and no further flexural cracks are developed along the length of the beam. Further, during negative cycles, beam top bars yielded and the strain dropped along length of the beam beyond drift ratio of -2.2%, as shown in Fig. 7, i.e., till the commencement of joint degradation. As there is no transverse reinforcement in the joint region of SP1, the entire shear resistance of joint completely relies on the diagonal strut that could not sustain under greater demand. However, the proper strut mechanism is mobilized up to the yielding of beam top
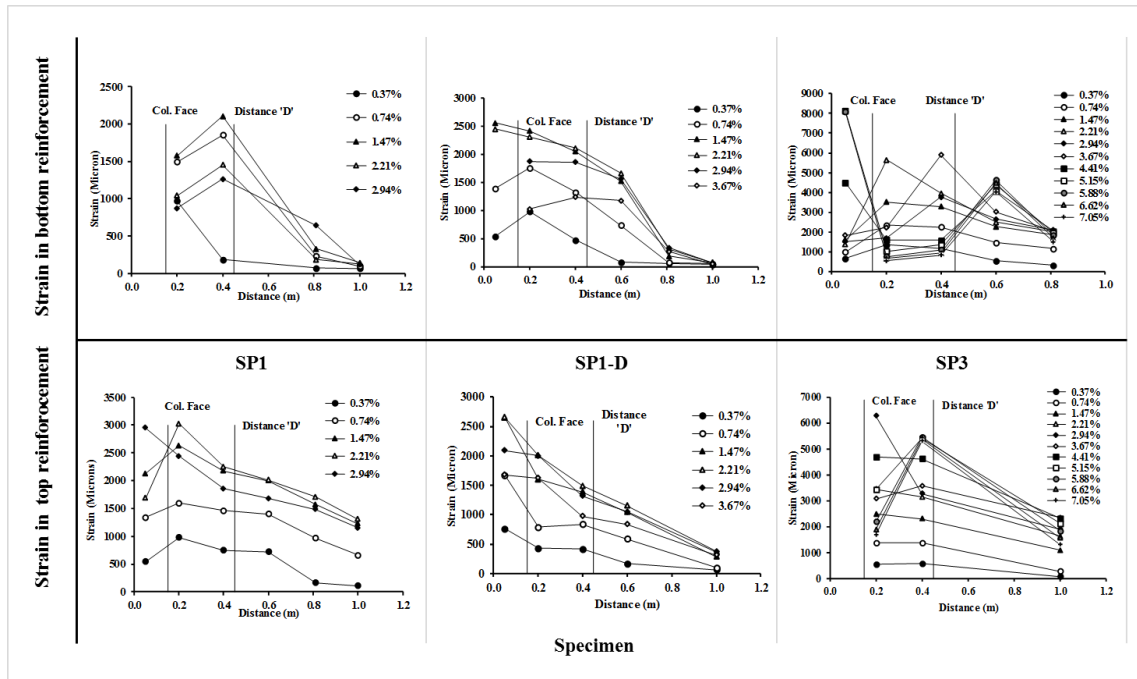
Fig. 7 Strain profile of top reinforcement (Negative cycle) and bottom reinforcement (Positive cycle) for different specimens

reinforcement in the gravity load designed specimen (SP1) under the negative cycle of loading which is not witnessed in the positive cycle of loading.

Unlike SP1, the anchorage failure of beam bottom bars did not happen in the case of SP1-D at the drift ratio of +1.47%, due to the compression anchorage provided to the bottom reinforcement. The yielding of beam reinforcement could be observed at the drift ratio of +1.47% at both top and bottom faces of beam from the strain recorded as shown in Fig. 7. Both beam top and bottom reinforcement bars of SP1-D developed almost same maximum strain, which could be observed from the strain records at distance of 0.05 m from the centre line of the column as shown in Fig. 7. Further, the strain gauges located up to the distance 'D' from the face of the column have also developed the strains till the drift ratio of 2.2%. With the commencement of the yielding of reinforcement, damage got shifted towards the joint as the joint did not possess enough shear resistance to cater for the huge shear demand imposed on the joint due to seismic type of loading. For specimen SP1-D, shear cracks along the diagonal connecting beam bottom and column outer (i.e., during negative cycle) are found to be more predominant compared to shear cracks developed in the positive cycle and propagated into the column region as shown in Fig. 6 due to formation of concrete diagonal strut. As the beam bottom reinforcements are provided with compression anchorage, the diagonal strut could not be completely developed along the other diagonal, which is showcased from the crack pattern observed in Fig. 6.

In specimen SP2, the flexural cracks developed along the beam are widened till drift ratio of +2.2% beyond which the flexural cracks in the beam remain dormant. After the drift ratio of +2.2%, the growth of joint shear crack is observed to be drastic, propagated into the column, and

extended beyond the depth of the column. During the final stage of loading i.e., at drift ratio of +5.88%, upheaving of concrete in the joint region and opening of joint is observed as shown in Fig. 6. In the present study, the strain profile of specimen SP2 under different drift ratios could not be established, as most of the strain gage signals are noisy. However, the strains would have reached the yield strain of reinforcement, as there is development of two prominent flexural cracks up to the drift ratio of +2.94% in the beam.

For specimen SP3, the flexural cracks are spread throughout the length of beam in both positive and negative cycles during initial drift increments. Two predominate cracks, one at the face of joint, and other at distance of D/2 from the face of joint are formed and widened during the positive cycles up to the drift ratio of 4.4%. Distance 'D' corresponds to the distance equal to the depth of the beam from the inner face of the column. Even though the diagonal shear cracks are developed at the drift ratio of +1.47%, the crack widths are smaller and the widening and propagation of diagonal shear cracks are active after the drift ratio of +4.4% and -3.67% in the positive and negative cycles respectively. At the final stage of loading, column cover concrete at the outer face of column spalled-off and upheaving of joint concrete is also observed as shown in Fig. 6 due to excessive shear deformation of joint region. From strain profiles of specimen SP3 during positive cycles, consistent development and shifting of yield peaks under different drift ratios could be witnessed as can be seen from Fig. 7. Even the strain gauge located at the distance of 0.8 m from the centre line of the column reached the yield strain, which is not observed in the other specimens tested. Thus, the confinement provided by stirrups facilitated the propagation of yield zone up to the drift ratio of 5.14% beyond which the strain dropped due to damage progression
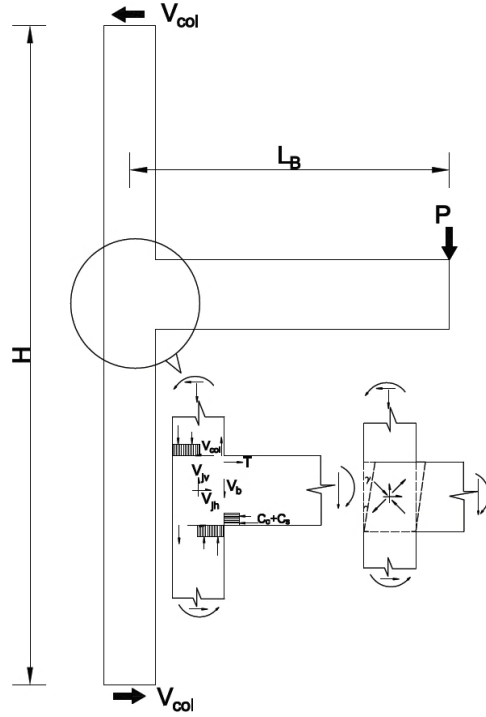
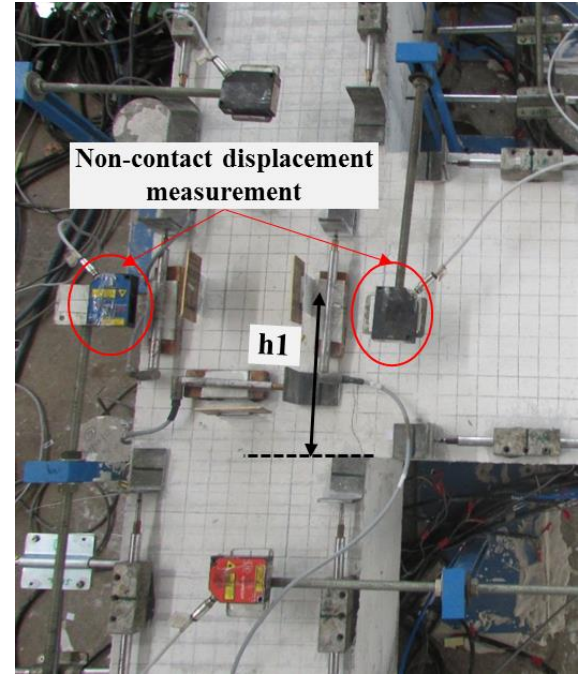Fig. 8(a) Force flow in exterior beam column sub-assemblage

Fig. 8(b) Instrumentation scheme to measure shear deformation

in the form of joint shear cracks. During the negative cycles of loading, the strains sustained up to the drift ratio of 4.4% beyond which the strains dropped due to the excessive joint damage. It is worthy to mention here that after the yield strain, the strain is found to drop because the main damage region is shifted from beam to the joint region which is also evident from damage patterns shown in Fig. 6.

It is interesting to note that specimen SP1-D performed better compared to gravity load designed specimen SP1. Though the gravity load design guidelines are lacking in providing proper anchorage to beam bottom reinforcement, a simple compression anchorage to the beam bottom reinforcement (even though they are not provided with anchorage required for moment at bottom face of beam) had facilitated a proper force transfer. It is also found from the experimental studies that with the evolution of the code provisions from gravity load designed to non-ductile and then to ductile specimens, a marked improvement in damage resilience is observed. From experimental investigation of Non-ductile (SP2) and ductile (SP3) specimens, it is noted that with appropriate reinforcement detailing and proper confinement, damage can be initially concentrated in beam portion and the joint deterioration can be delayed to an extent. Further, it is noted that in all the specimens except SP1 the damage progression is through beam cracking (due to yielding of reinforcement) followed by joint cracking and no damage to columns was witnessed. Hence, the joint strengthening or providing alternate force path to reduce the joint shear damages would result in desired flexural mode of failure. In the case of SP1, the anchorage failure of beam bottom reinforcement resulted in the sudden load drop and hence the GLD structures need

immediate retrofit intervention to prevent severe damage under seismic event.

4.2 Joint shear deformation

Under the action of lateral loading, force flow that exists in an exterior beam column sub-assemblage is as shown in the Fig. 8(a). The horizontal shear force acting in the joint is given by

$$V_{jh} = T - V_{col} \qquad (2)$$

Where V_{jh} - horizontal joint shear acting at the center of the joint; T- tension in the beam top reinforcement bars

$$T = \frac{PL_b}{z} \qquad (3)$$

From the force equilibrium of beam column sub-assemblage, the column shear V_{col} is given by

$$V_{col} = \frac{PL_b}{H} \qquad (4)$$

Where P is the beam tip load; L_b is the distance from centre of the column to the inflection point of the beam; H is the height of the column. z - lever arm between the resultant beam compression and tensile forces. The lever arm distance is assumed as $0.9d$ where d is the distance from the beam extreme compression fibre to the centroid of the tension reinforcement in the present study. The horizontal nominal shear stress (v_{jh}) in the joint region is given as below

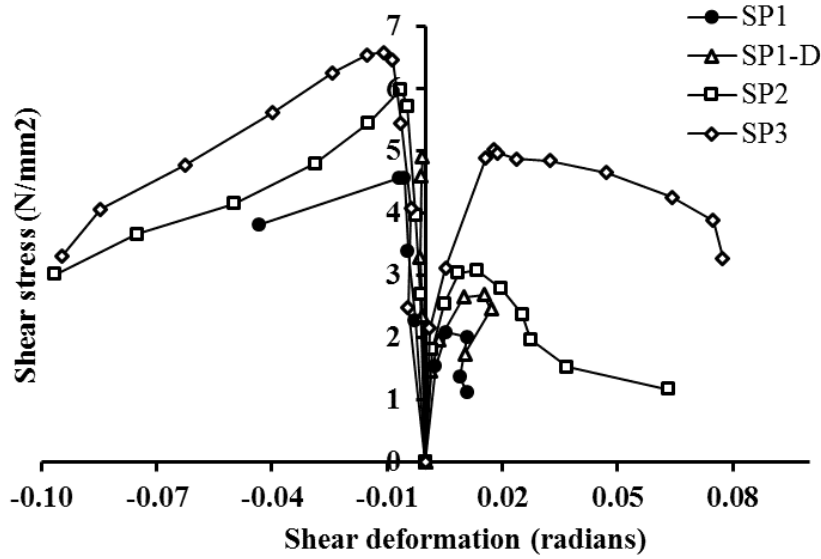$$v_{jh} = \frac{V_{jh}}{b_w h} \qquad (5)$$

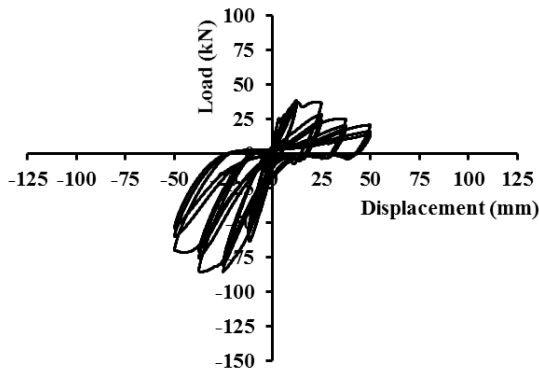Fig. 9 Nominal joint shear stress versus joint shear deformation

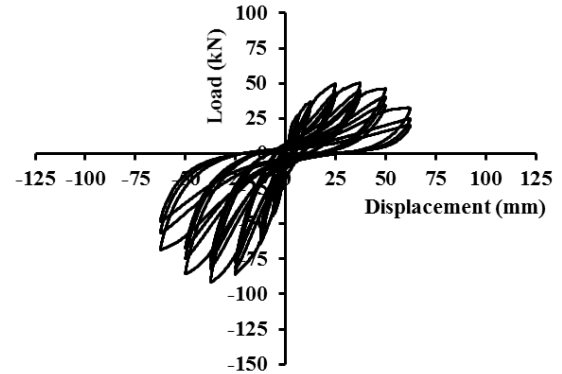Fig. 10(a) Load -displacement hysteresis of SP1

Fig. 10(b) Load -displacement hysteresis of SP1-D

Where h is the overall depth of the beam and effective joint width (b_w) shall not exceed the smaller of (a) beam width plus joint depth (b) twice the smaller perpendicular distance from longitudinal axis of beam to column side. (ACI 318M 2011)

The shear deformation angle (γ) as shown in the Fig. 8(a) is measured using non-contact optical (LASER) based measurement. The instrumentation scheme adopted in the present study to measure shear deformation angle is as shown in Fig. 8(b). The stainless steel plate of thickness 2 mm and depth equal to the cover concrete and projection of 60 mm above the joint concrete was inserted into the joint region at the time of casting of specimens. Plywood sheets are glued to the projected surface of the stainless steel plate. The distance of the non-contact measurement point (h_1) from the bottom face of joint was measured prior to the experimental investigation and the deformation Δ_1 during the test is measured using the non-contact measurements. Thus, the shear deformation angle could be obtained as given below

$$\text{Shear deformation angle, } \gamma = \frac{\Delta_1}{h_1} \qquad (6)$$

Shear deformation of the joint versus nominal shear

stress calculated according to Eq. (5) is shown in Fig. 9. FEMA 273 (1997) provides the acceptance criteria for shear deformation angle of conforming and non-conforming reinforced concrete exterior beam-column joints as 0.01 and 0.005 respectively. The seismic load designed specimens SP2 and SP3 satisfy the acceptance criteria. During positive drift cycles, the shear deformation of SP1 is found to be very small compared to other three specimens due to the anchorage failure of beam bottom reinforcement. For Specimen SP1-D, as the joint cracks are opened up, the measurement reference point got disturbed and the shear deformation at drift ratios greater than +2.21% could not be obtained. Even though the size of joint remains same for all the four specimens, SP3 showed remarkable shear resistance due to the confinement effect provided by the transverse reinforcement in the joint region. During negative cycle, the shear deformation increases with the increase in drift ratio and the specimens exhibited global strength degradation behavior.

4.3 Load-displacement behavior

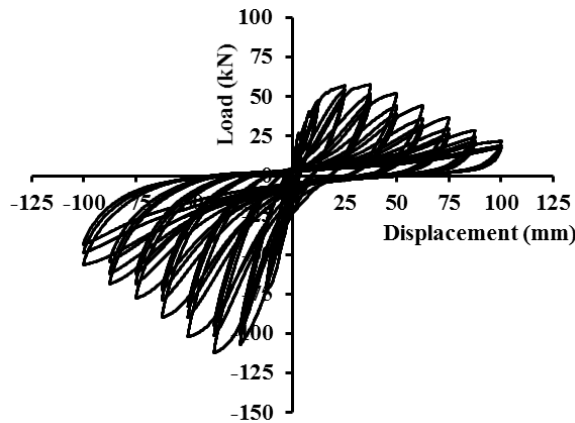The load versus displacement hysteresis curves obtained

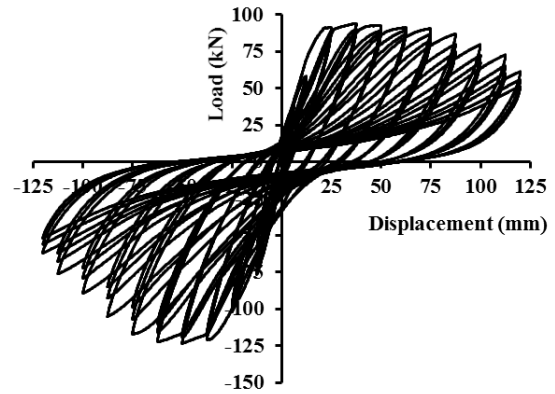Fig. 10(c) Load -displacement hysteresis of SP2

Fig. 10(d) Load -displacement hysteresis of SP3

from reverse cyclic tests carried out on specimens SP1, SP1-D, SP2 and SP3 are shown in Figs. 10(a)-(d) respectively.

From the load-displacement hysteresis curves, it is evident that specimen SP1, which is designed only for gravity loads exhibited poor seismic performance when compared to that of the other specimens. The poor seismic performance of specimen SP1 is due to lack of anchorage and inadequate reinforcement at beam bottom. The maximum load carried by specimen SP1 during the positive cycles is 46% of the maximum load carried by the same specimen during the negative cycles. In the positive cycle of specimen SP1, the load is dropped at the displacement cycle of 25 mm (1.47% drift ratio) due to the slippage of beam bottom reinforcement, which could be witnessed by the formation of a prominent wide crack at the joint. During negative cycle of loading on specimen SP1, the load increases with the increase in displacement until the yielding of beam top reinforcement had taken place. Beyond this, with the further increase of drift, degradation in global strength is observed due to joint damage.

Specimen SP1-D showcased better performance compared to that of SP1 as the yielding of beam reinforcement occurred in both positive and negative cycles of SP1-D and the load drop is noted only after 37.5 mm (i.e., -2.2%) drift cycle. Up to the displacement of 12.5 mm, maximum load carried by SP1 and SP1-D are almost same. The maximum load carried by SP1-D in positive and negative cycles is 29% and 7% higher than that of SP1 respectively. Even though specimen SP1-D is designed only for gravity loads, it had demonstrated far better performance under reverse cyclic loading compared to specimen SP1, because the beam bottom reinforcement in SP1-D is provided with compression anchorage unlike straight bar in case of SP1. In fact, performance of SP1-D is comparable with that of SP2, which is designed for seismic loads in terms of load carrying capacity. For specimen SP2, the load values increased with the increase in drift till the yielding of both top and bottom beam reinforcement bars had taken place. After the yielding of steel, specimen exhibited strength degradation due to severe damage in joint region during both positive and negative load cycles. The maximum load carried by SP2 in both positive and negative

cycles is 15% and 22% higher than that of SP1-D as can be seen from Figs. 10(b) and 10(c). Hence, the specimen SP1-D may sustain moderate seismic risk or design basis earthquake but cannot sustain extreme seismic event. In fact, the specimen SP1-D and SP2 had same top and bottom beam reinforcement, the only difference between them is the anchorage of beam bottom reinforcement (SP1-D had compression anchorage for beam bottom bars and SP2 had anchorage for beam bottom bars to cater to the moment at that face at the joint) but specimen SP2 endured larger drift cycles when compared to SP1-D. The presence of intermediate column bars and proper anchorage of beam bottom reinforcement facilitated better performance of SP2. Specimen SP3 (with ductile detailing) carried more load than SP2 [Fig. 10(d)] even though it is designed for lesser seismic force (as response reduction factor for SP2 and SP3 are 3 and 5 respectively). In the positive cycle, the maximum strength is attained in SP3 at a displacement level of 37.5 mm (drift of 2.2%) and the load is sustained up to the displacement level of 87.5 mm (drift of 5.15%). This may be due to the presence of confinement of joint due to presence of ties in the joint region. Beyond this displacement level, strength degradation is observed. In negative cycles of SP3, after attaining the maximum strength at drift ratio of 2.2% the load sustained for subsequent displacement levels (from drift ratio of 2.2% to 3.68%) and then strength begins to decrease. The load displacement hysteresis is unsymmetrical for positive and negative cycles in all the four specimens since the beam main reinforcement at the top and bottom are unequal.

The load-displacement backbone curves obtained for all the four specimens are shown in Fig. 11. The maximum loads carried by the specimens SP1, SP1-D, SP2 and SP3 in the positive cycle are 39 kN, 50 kN, 58 kN and 94 kN respectively. The higher load carried by ductile detailed specimen is due to provision of additional steel reinforcement at the beam bottom in the view of ductility detailing (positive steel at the face of the joint should be at least 50% of the negative steel (IS 1893 2002)). In the negative cycle, maximum load carried by specimens SP1, SP1-D, SP2 and SP3 are 85 kN, 91 kN, 112 kN and 123 kN, respectively. Even though specimen SP2 has slightly higher reinforcement than specimen SP3 at beam top, SP3 carried
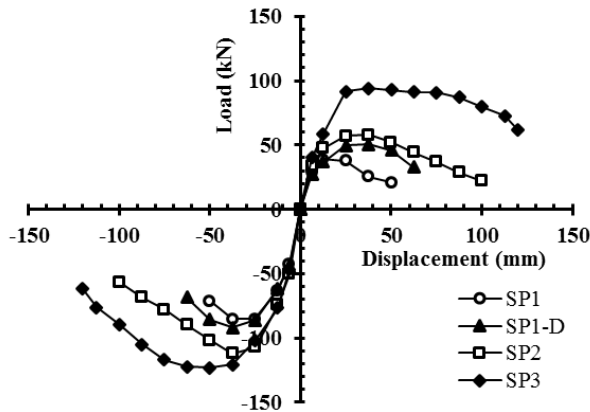
Fig. 11 Load Envelope of specimens SP1, SP1-D, SP2 and SP3

Fig. 12 Global strength degradation of specimens with progression of drift ratio

higher load than the non-ductile specimen. This could be due to the fact that proper force transfer mechanism took place in ductile detailed specimen from beam to column through joint and also reduced degradation of joint due to confinement of joint provided by the ductility detailing of joint region. The maximum load carried by SP3 in the positive cycle is 141%, 87%, and 63% higher than that of SP1, SP1-D, and SP2, respectively. Similarly, the maximum load carried by SP3 in the negative cycle is 44%, 34%, and 10% higher than that of SP1, SP1-D, and SP2 respectively. A tremendous improvement in the loading carrying capacity was observed in the specimen SP3 in both the positive and negative cycles compared to that of the deficient specimens. This signifies the importance and underlines the need for providing ductility detailing. However, even in specimen SP3 weak beam mode of failure is not observed and the specimen encountered joint shear failure. This may be probably due to the proportioning of member (namely beam and column) sizes, and the detailing practices adopted according to Indian code (IS: 13920 1993).

4.4 Global strength degradation and ductility

Degradation in global strength with the increment in drift ratio is as shown in Fig. 12. Strength degradation is evaluated considering load of first cycle of each drift ratio. It could be observed from Fig. 12 that the global strength degradation of all specimens except specimen SP1 occurred after the drift ratio of 2.2%. In specimen SP1, the global strength degradation occurred at drift ratio of 0.737% due to anchorage failure of beam bottom reinforcement. The global strength degradation increases with the increase in drift ratio for all the specimens. The level of degradation for ductile detailed specimen (SP3) is much smaller than that of non-ductile specimen (SP2) as can be seen in Fig. 12. It could be observed that global strength degradation of SP1-D and SP2 are same till the drift ratio of 2.94% and beyond that drift ratio the degradation of SP1-D is faster than that of SP2. Superior performance of ductile detailed specimen SP3 compared to all the evolutions of design is evident from Fig. 12. It is observed that the level of degradation is significantly dependent on the confinement provided rather
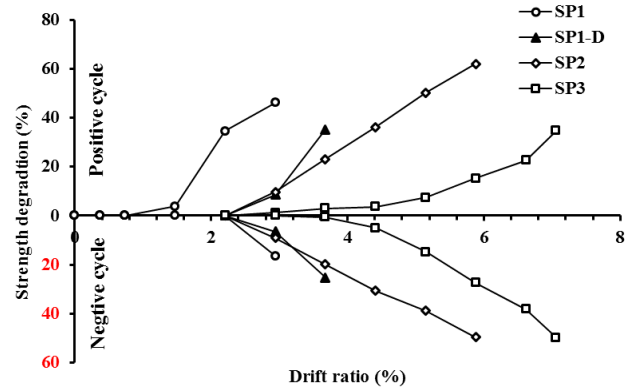
than on the area of main reinforcement provided. At drift ratio of +3.67%, the global strength degradation of SP3, SP2 and SP1-D is 3%, 23% and 35% respectively and at -3.67%, the global strength degradation is found to be 1%, 20% and 25% respectively.

The displacement ductility is defined as the ratio of post peak displacement corresponding to 85% of the ultimate load to that of the yield displacement (EC8 2004). Thus, the ductility is expressed as given in Eq. (7). Accordingly, the displacement ductility of the specimens are evaluated and presented in Table 4

$$\mu = \frac{\Delta_{max}}{\Delta_{yield}} \qquad (7)$$

Where, Δ_{max}= Post peak displacement corresponding to 85% of peak load; Δ_{yield}= displacement corresponding to yielding of steel

From the Table 4, it may be noted that even the cases of seismically designed specimens SP2 and SP3 do not attain the expected ductility [according to Eq. (7)] requirement of 3 and 5 respectively. However, from Fig. 12 it may be noted that SP2 attains the ductility of 3 i.e., between drift ratio of +1.47% (at which yielding of reinforcement is observed) and +4.41% with the global strength degradation of 36% and 30% in the positive and negative cycles respectively. Similarly, specimen SP3 attains the displacement ductility of 5 from drift ratio of 1.47% (at which yielding of reinforcement is observed) to 6.61% with the global strength degradation of 22% and 38% in the positive and

Table 4 Displacement ductility of specimens

ID	Ductility (μ) (positive cycle)	Ductility (μ) (negative cycle)	$R = \dfrac{\text{Design load}}{\text{Elastic response load}}$	Expected Ductility $\mu_e = 1/R$
SP1	Bars not yielded	2	NA	NA
SP1-D	2	2	NA	NA
SP2	2	2	0.33	3
SP3	4	3.5	0.2	5

negative cycles respectively. Thus, the seismically designed specimens are vulnerable to joint shear failure and needs strengthening of joint to sustain larger earthquakes than the design basis earthquakes.

4.5 Energy dissipation

The energy dissipation is one of the crucial seismic performance parameters, as the energy imparted to system during earthquake has to be dissipated either elastically or through elastic-plastic response. As most of the seismic design principles rely on the inelastic deformation of the structure to withstand severe earthquakes, it is highly essential to ensure the required energy dissipation to prevent collapse of structures during severe earthquake. The cumulative energy dissipation capacities of specimens SP1, SP1-D, SP2 and SP3 are shown in Fig. 13. The specimens SP1 and SP1-D dissipated almost same amount of energy until the drift ratio of 2.2% but at the drift ratio of 2.94%, cumulative energy dissipated by SP1 is 13% lower than that of SP1-D. The total cumulative energy dissipated by specimen SP1-D is 1.58 times that of SP1. Further, SP1-D sustained deformation up to drift ratio of 3.67%. The prevention of anchorage failure of beam bottom bars in SP1-D showcased better energy dissipation compared to specimen SP1. Even though the maximum load carried SP1-D is comparable to SP2, the total cumulative energy dissipated by SP2 is 2.39 times higher that of SP1-D. It signifies that the strength and energy dissipation are two independent parameters for seismic performance assessment and needs to be evaluated separately. It is important to mention here that under moderate earthquake higher strength of the structure is required, whereas a severe earthquake demands higher ductility. Hence, the specimen SP1-D may sustain the moderate seismic risk even though they could not sustain larger drift unlike SP2. Further, provision of proper anchorage of bottom beam reinforcements in the case of specimen SP2 produced phenomenal improvement in the energy dissipation of the specimen. Till the drift ratio of 2.2%, the cumulative energy is same for the specimens SP1, SP1-D and SP2. Beyond this drift ratio, SP2 dissipated more energy through large inelastic deformation, which is absent in both the gravity load designed specimens SP1-D and SP1. The total cumulative energy dissipated by the specimens SP1, SP1-D, SP2 and SP3 is found to be 11.65 kNm, 18.45 kNm, 44.10 kNm and 113.33 kNm respectively. The provision of ductility detailing in the specimen SP3 improved its energy dissipation tremendously. The specimen SP3 which had nearly same quantity of total reinforcement (for the sub-assemblage as whole) as that of SP2 showcased tremendous improvement in the energy dissipation capacity of nearly 2.56 times that of SP2. Furthermore, the gravity load designed specimens SP1 and SP1-D respectively dissipated only one tenth and one sixth of the energy dissipated by SP3. This signifies the superior performance of ductile detailed specimen SP3 and deficiency of GLD specimens. Thus, with proper confinement and appropriate detailing practice, energy dissipation improved drastically.
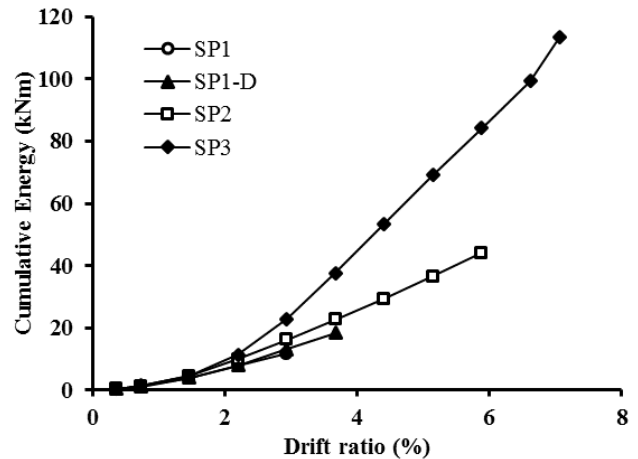
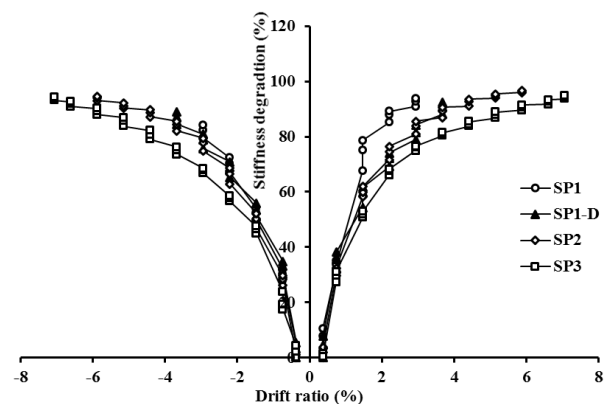

Fig. 13 Cumulative energy dissipation

Fig. 14 Stiffness Degradation of all the specimens

4.6 Stiffness degradation

The stiffness degradation of all the specimens is shown in Fig. 14. Large stiffness degradation is observed during the positive cycles of SP1 when compared to other specimens due to separation at the joint. Under same drift level of the negative cycle, SP1 showed nearly equal stiffness degradation as that of SP1-D and SP2. The specimens SP1-D and SP2 showed almost same stiffness degradation in both positive and negative cycles, whereas in positive cycle SP1 has undergone much higher stiffness degradation after the anchorage failure of rebar. Specimen SP3 showed lesser stiffness degradation compared to all the other specimens considered in the present study. At drift ratio of 2.2%, stiffness degradation in first positive cycle of SP3 is 8%, 9%, 29% lower than that of SP2, SP1-D and SP1 respectively. In the corresponding negative cycle, stiffness degradation in SP3 is 11%, 15% and 18% lower than that of SP2, SP1-D and SP1 respectively. It is also observed that stiffness degradation in the positive cycles is more than the stiffness degradation in the negative cycles for all the specimens. At drift ratio of 2.2%, stiffness degradation in first positive drift cycle is 14%, 12%, 10% and 21% lower than that in the corresponding negative drift cycle of SP3, SP2, SP1-D and SP1 respectively. Before failure, the specimens exhibited severe damage in the form of flexural cracks, shear cracks in the joint region and up-

Table 5 Strength degradation of specimens

Drift ratio	Strength Degradation (%) in positive cycle				Strength Degradation (%) in negative cycle			
	SP1	SP1-D	SP2	SP3	SP1	SP1-D	SP2	SP3
0.37(1)	0.0	0.0	0.0	0.0	0.0	0.0	0.0	0.0
0.37(2)	8.3	5.2	1.9	1.3	3.8	3.5	0.4	2.1
0.37(3)	10.9	8.3	3.9	0.4	5.1	5.6	1.2	4.7
0.74(1)	0.0	0.0	0.0	0.0	0.0	0.0	0.0	0.0
0.74(2)	4.1	4.9	1.5	3.2	3.0	4.6	3.1	2.3
0.74(3)	4.1	8.2	3.9	5.2	5.8	6.9	4.6	7.2
1.47(1)	0.0	0.0	0.0	0.0	0.0	0.0	0.0	0.0
1.47(2)	23.9	11.9	4.1	2.3	5.4	4.5	6.4	2.9
1.47(3)	34.5	16.0	9.1	4.1	8.3	9.9	10.1	4.6
2.21(1)	0.0	0.0	0.0	0.0	0.0	0.0	0.0	0.0
2.21(2)	18.5	10.0	10.1	3.9	10.5	10.7	9.7	2.8
2.21(3)	26.9	15.9	16.9	5.5	16.3	16.4	15.6	4.6
2.94(1)	0.0	0.0	0.0	0.0	0.0	0.0	0.0	0.0
2.94(2)	20.5	12.4	15.1	4.0	14.1	12.6	12.2	3.2
2.94(3)	31.0	25.3	24.5	5.4	23.1	21.4	18.9	5.1
3.68(1)	-	0.0	0.0	0.0	-	0.0	0.0	0.0
3.68(2)	-	23.2	18.4	2.0	-	17.3	12.0	5.2
3.68(3)	-	37.3	27.6	4.7	-	29.3	19.5	9.8
4.41(1)	-	-	0.0	0.0	-	-	0.0	0.0
4.41(2)	-	-	18.9	4.0	-	-	12.1	8.4
4.41(3)	-	-	28.1	8.7	-	-	19.8	15.6
5.15(1)	-	-	0.0	0.0	-	-	0.0	0.0
5.15(2)	-	-	14.3	8.0	-	-	9.6	11.8
5.15(3)	-	-	24.1	14.3	-	-	20.5	19.0
5.88(1)	-	-	0.0	0.0	-	-	0.0	0.0
5.88(2)	-	-	13.0	8.8	-	-	13.6	11.2
5.88(3)	-	-	18.4	15.2	-	-	23.0	19.0
6.62(1)	-	-	-	0.0	-	-	-	0.0
6.62(2)	-	-	-	9.9	-	-	-	11.0
6.62(3)	-	-	-	16.8	-	-	-	18.7
7.06(1)	-	-	-	0.0	-	-	-	0.0
7.06(2)	-	-	-	8.9	-	-	-	9.5
7.06(3)	-	-	-	15.8	-	-	-	16.6

heaving of concrete in the joint region due to excessive shear deformation and leading to huge stiffness degradation. It is essential to highlight that the four specimens SP1, SP1-D, SP2 and SP3 suffered more than 90% of stiffness degradation before failure in both positive and negative cycles, but this had happened at different drift levels i.e., with the evolution of level of design of the specimens the stiffness degradation is delayed.

4.7 Strength degradation within the cycles of the same drift ratio

Fig. 15 and Table 5 gives the strength degradation during the second and third cycles with respect to the first cycle of each drift ratio.

In specimen SP1, maximum strength degradation of 35% is observed between first and third cycles at drift ratio of 1.47% due to the anchorage failure of beam bottom reinforcement during positive cycles. Whereas during negative cycles maximum strength degradation of 23% occurred between first and third cycles at the drift ratio of 2.94%. For SP1-D, the maximum strength degradation of 37.3% and 29.3% is observed at the drift ratio of 3.68% in both positive and negative cycles respectively. The maximum strength degradation of 28% and 23% occurred between first and third cycles at the drift ratio of +4.41%
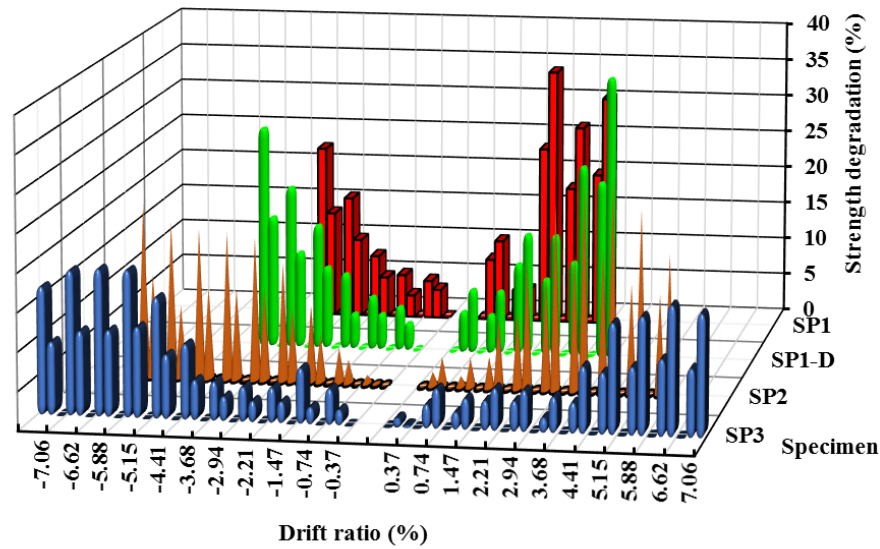
Fig. 15 Strength Degradation of all the specimens

and -5.88%, respectively in specimen SP2. For SP3, the maximum strength degradation of 16.8% and 18.7% occurred between first and third cycles at the drift ratios of +6.62% and -6.62% respectively. Thus, it could be observed that damage progression is delayed with the evolution of specimens. From Fig. 15 and Table 5, it is observed that the strength degradation in the positive cycles is larger than that in the negative cycles for all the specimens except SP3. Specimen SP3 showed slightly higher strength degradation in negative cycles compared to that in the positive cycles. For all the specimens, it is found that the strength degradation between first and second cycles is larger compared to the strength degradation between second and third cycles. Even though SP2 is designed for higher seismic forces than SP3 (as response reduction factors for SP2 and SP3 are 3 and 5 respectively), the strength degradation of SP2 is much larger than that of SP3 in both positive and negative cycles during lower drift ratios. The strength degradation of SP3 is lesser than that of the other specimens in both positive and negative cycles. Further, during the positive cycles of loading, strength degradation of SP3 is less than 10% up to the drift ratio of +4.4% as long as the load is sustained. At drift ratio of +1.47%, the strength degradation between first and third cycles is found to be 35%, 16%, 9%, and 4%, for specimens SP1, SP1-D, SP2, and SP3 respectively. Similarly, under negative cycle of loading at drift ratio of 1.47%, the strength degradation between first and third cycles is found to be 8%, 10%, 10%, and 5% for SP1, SP1-D, SP2, and SP3 respectively. Thus, the ductile detailing and resulting confinement in SP3 reduced the strength degradation within the cycles of same drift level.

5. Conclusions

The primary focus of the paper is to experimentally evaluate the seismic performance of beam-column sub-assemblages designed according to different levels of design that represent the evolution of design for RC structures during last 4-5 decades. In the present study, performance of four types of specimens viz., i) Gravity load designed with straight bar anchorage (SP1), ii) Gravity load designed with compression anchorage (SP1-D), iii) designed for seismic force but not provided with ductility detailing (SP2), and iv) designed for seismic force and provided with ductility detailing (SP3) are assessed experimentally under reverse cyclic loading. From the experimental investigations and the results obtained, the following conclusions are drawn:

• With the evolution of the code provisions from gravity load designed to non-ductile and then to ductile specimens, a marked improvement in damage resilience is observed.

• It is observed that the specimen SP1 which is designed only for gravity loads exhibited poor seismic performance when compared to the other specimens due to lack of anchorage and inadequate reinforcement at beam bottom. The anchorage failure of beam bottom reinforcement resulted in the sudden load drop.

• Specimen SP1-D showed better performance compared to specimen SP1, as the yielding of beam reinforcement occurred in both positive and negative cycles. Even though specimen SP1-D is designed only for gravity loads, it has demonstrated better performance under reverse cyclic loading and is comparable with that of SP2 (designed for seismic loads) in terms of maximum load carrying capacity. Hence, the specimen SP1-D may sustain moderate seismic risk or design basis earthquake but cannot sustain extreme seismic event.

• In all the specimens except SP1 the damage progression is through beam cracking followed by joint cracking and no damage to column was witnessed.

Hence, the joint strengthening or providing alternate force path to reduce the joint shear demand would result in desired flexural mode of failure.

• The maximum load carried by SP3 in the positive cycle is 141%, 87%, and 63% higher than that of SP1, SP1-D, and SP2, respectively. Similarly, the maximum load carried by SP3 in the negative cycle is 44%, 34%, and 10% higher than that of SP1, SP1-D, and SP2 respectively. Tremendous improvement in the load carrying capacity was observed in the specimen SP3 in both positive and negative cycles compared to that of the deficient specimens.

• The gravity load designed specimens SP1 and SP1-D respectively dissipated only one-tenth and one-sixth of the energy dissipated by SP3. The specimen SP3 which had nearly same quantity of total reinforcement (for the sub-assemblage as whole) as that of SP2 showcased tremendous improvement in the energy dissipation capacity of nearly 2.56 times that of SP2.

• From the strength degradation behavior of specimens SP2 and SP3, it is observed that the magnitude of strength degradation depends upon level of confinement provided in the joint region rather than on the quantity of beam main reinforcement.

• It is essential to highlight the fact that even the specimens SP2 and SP3 do not attain the expected ductility of 3 and 5 respectively at strength degradation of 15% as defined by EC8(2004). However, they found to satisfy the ductility requirement at strength degradation of about 30% as the joint shear degradation reduces the deformation capacity. Thus, strengthening of joint or reducing the shear demand on the joint assumes importance for sustaining large earthquakes.

• From the seismic performance of specimens, it could be observed that existing buildings which were designed according to the then prevailed standards need joint strengthening or alternate force flow path mechanism which would reduce the joint shear demand in order to sustain larger seismic events. Further, specimen SP1 showed sudden anchorage failure which necessitates immediate seismic interventions in order to avoid catastrophic collapse of GLD structures of similar detailing. Thus, the insight from the present study would be useful for formulating seismic strengthening/retrofit measures to the deficient RC structures similar to that chosen for study.

Acknowledgments

References

ACI 318M (2011), Building Code Requirements for Structural Concrete and Commentary, Farmington Hills, MI, USA.

Aycardi, L.E., Mander, J.B. and Reinhorn, A.M. (1994), "Seismic resistance of reinforced concrete frame structures designed only for gravity loads: Experimental performance of sub-assemblages", *ACI Struct. J.*, **91**(5), 552-563.

Bakir, P.G. (2003), "Seismic resistance and mechanical behaviour of exterior beam-column joints with crossed inclined bars", *Struct. Eng. Mech.*, **16**(4), 493-517.

Bindhu, K.R., Jaya, K.P. and Manicka Selvam, V.K. (2008), "Seismic resistance of exterior beam-column joints with non-conventional confinement reinforcement detailing", *Struct. Eng. Mech.*, **30**(6), 733-761.

Blakeley, R.W.G., Megget, L.M. and Priestley, M.J.N. (1975), "Seismic performance of two full size reinforced concrete beam-column joint units", *Bull. NZ. Nat'l Soc. Earthq. Eng.*, **8**(1), 38-69.

Bracci, J.M., Reinhorn, A.M. and Mander, J.B. (1995), "Seismic resistance of reinforced concrete frame structures designed for gravity loads: performance of structural system", *ACI Struct. J.*, **92**(5), 597-609.

Calvi, G.M., Magenes, G. and Pampanin, S. (2002), "Experimental test on a three storey RC frame designed for gravity only", *12th European Conference on Earthquake Engineering*, September, London.

Chun, S.C. (2014), "Effects of joint aspect ratio on required transverse reinforcement of exterior joints subjected to cyclic loading", *Earthq. Struct.*, **7**(5), 705-718.

Dhakal, R.P., Pan, T.C., Irawan, P., Tsai, K.C., Lin, K.C. and Chen, C.H. (2005), "Experimental study on the dynamic response of gravity-designed reinforced concrete connections", *Eng. Struct.*, **27**(1), 75-87.

Ehsani, M.R. and Wight, J.K. (1985), "Exterior reinforced concrete beam to column connections subjected to Earthquake - type loading", *ACI Struct. J.*, **82**(4), 492-499.

El-Attar, A.G., White, R.N. and Gergely, P. (1997), "Behaviour of gravity load designed reinforced concrete buildings subjected to earthquakes", *ACI Struct. J.*, **94**(2), 133-145.

EC8 (2004), Design of structures for earthquake resistance - Part 1: General rules, seismic actions and rules for buildings, European committee for standardization, Brussels, Belgium.

FEMA 273 (1997), "Guidelines for the seismic rehabilitation of buildings", Federal Emergency Management Agency, Washington, D.C., USA.

IS 1893(2002), Criteria for earthquake resistant design of structures (Part 1): General provisions and buildings, Bureau of Indian Standards, New Delhi, India.

IS 456(2000), Code of practice for plain and reinforced concrete (Fourth revision), Bureau of Indian Standards, New Delhi, India.

IS 13920 (1993), Ductility detailing of reinforced concrete structures subjected to seismic forces, Bureau of Indian Standards, New Delhi, India.

Masi, A., Santarsiero, G., Lignola, G.P. and Verderame, G.M. (2013), "Study of the seismic behaviour of external RC beam-column joints through experimental tests and numerical simulations", *Eng. Struct.*, **52**, 207-219.

Marthong, C., Deb, S.K. and Anjan Dutta (2016), "Experimental fragility functions for exterior deficient RC beam-column connections before and after rehabilitation", *Earthq. Struct.*, **10**(6), 1291-1314.

Megget, L.M. and Park, R. (1971), "Reinforced concrete exterior beam-column joints under seismic loading", *NZ. Eng.*, **26**(11), 341-353.

Murty, C.V.R, Rai, D.C., Bajpai, K.K. and Jain S.K. (2003), "Effectiveness of reinforcement details in exterior reinforced concrete beam-column joints for earthquake resistance", *ACI Struct. J.*, **100**(2), 149-156.

NZS 3101(2006), Concrete Structures Standard Part 1 -The

Design of Concrete Structures, Standards New Zealand, Wellington, New Zealand.

Pantelides, C.P., Hansen, J., Nadauld, J. and Reaveley, L.D. (2002), "Assessment of reinforced concrete building exterior joints with substandard details", PEER Report 18, University of California, Berkeley.

Park, R. and Paulay, T. (1973), "Behaviour of reinforced concrete external beam column joints under cyclic loading", *Proceedings of Fifth World Conference on Earthquake Engineering*, 1, 772-781.

Park, R. and Yeoh Sik Keong (1979), "Tests on structural concrete beam-column joints with intermediate column bars", *Bull. NZ. Nat'l Soc. Earthq. Eng.*, **12**(3), 2361-2376.

Paulay, T. and Scarpas, A. (1981), "The behaviour of exterior beam-column joints", *Bull. NZ. Nat'l Soc. Earthq. Eng.*, **14**(3), 131-144.

Paulay, T., Park, R. and Priestley, M.J.N. (1978), "Reinforced concrete beam-column joints under seismic actions", *Proceedings Journal of the American Concrete Institute*, **75**(11), 585-593.

Rajagopal, S. and Prabavathy, S. (2013), "Study of exterior beam-column joint with different joint core and anchorage details under reversal loading", *Struct. Eng. Mech.*, **46**(6), 809-825.

Supaviriyakit, T. and Pimanmas, A. (2008), "Comparative performance of sub-standard interior reinforced concrete beam-column connection with various joint reinforcing details", *Mater. Struct.*, **41**(3), 543-557.

Somma, G., Pieretto, A., Rossetti, T. and Grant, D.N. (2015), "R.C. beam to column connection failure assessment and limit state design", *Mater. Struct.*, **48**(4), 1215-1231.

Tsonos, A.G. (2007), "Cyclic load behavior of reinforced concrete beam-column sub-assemblages of modern structures", *ACI Struct. J.*, **104**(4), 468-478.

Yavari, S., Elwood, K.J., Wu, C.L., Lin, S.H., Hwang, S.J. and Moehle, J.P. (2013), "Shaking table tests on reinforced concrete frames without seismic detailing", *ACI Struct. J.*, **110**(6), 1001-1012.

AG